Reactivity of an Fe^{IV}–Oxo Complex with Protons and Oxidants

Ethan A. Hill,[§] Andrew C. Weitz,[¶] Elizabeth Onderko,[‡] Adrian Romero-Rivera,[‖] Yisong Guo,[¶*] Marcel Swart,[‖,#*] Emile L. Bominaar,[¶*] Michael T. Green,[§*] Michael P. Hendrich,[¶*] David C. Lacy,[§,†*] A. S. Borovik[§*]

[§]Department of Chemistry, University of California-Irvine, 1102 Natural Sciences II, Irvine, CA 92697

[¶]Department of Chemistry, Carnegie Mellon University, Pittsburgh, PA 15213

[‡]Department of Chemistry, Pennsylvania State University, University Park, PA 16802

[‖]Institut de Química Computacional i Catàlisi & Dept. Química, Universitat de Girona, Spain

[#]ICREA, Pg. Lluís Companys 23, 08010 Barcelona, Spain

Contents

General Procedures and experimental details S1

Table S1. Best fit for EXAFS data. S10

Table S2. Best fits for Fourier filtered EXAFS data. S10

Table S3. DFT determined Properties for the **1a-1c**. S10

Figure S1. Mössbauer, EPR, and optical spectra of **2** from deprotonation S11

Figure S2. UV-vis spectra of the comproportionation of **1** with **3** S11

Figure S3. EPR spectra of the comproportionation of **1** with **3** S12

Figure S4. EPR spectrum of the reduction of **1** with [$CoCp_2$] S12

Figure S5. XANES spectra for **1**, **2**, and **4**. S13

Figure S6. EXAFS data and the Fourier transforms for **1**, **2**, and **4**. S14

Figure S7. Fourier filtered EXAFS data and the Fourier transforms for **1**, **2**, and **4**. S15

Figure S8. Cyclic voltammogram of **2** in THF S16

Figure S9. Mössbauer spectra of **1** prepared by oxidation of **2** S16

Figure S10. Experimental evidence for the reaction shown in eq 3. S17

Figure S11. UV-vis spectrum of **9** S17

Figure S12. Gas chromatogram of oxidation of **2** in the presence of **8** S18

Figure S13. GC-MS data of the oxidation of **2** in the presence of **8** S19

Figure S14. Optical results from control experiments S19

References S20

General Procedures All manipulations, unless otherwise stated, were performed under an argon atmosphere in a Vac-atmospheres dry box. All chemicals were purchased from commercial sources and used without further purification unless otherwise stated. $K[Fe^{IV}H_3buea(O)]$, $K[Fe^{III}H_3buea(OH)]$, $K_2[Fe^{II}H_3buea(OH)]$, and [N(*p*-tolyl)$_3$][OTf] were prepared according to previously published procedures.[1–4]

General Procedure for Synthesis of Acids. A modified procedure for the synthesis of the conjugate acid of an amine was followed for all acids.[5] A solution of amine in diethyl ether was cooled to 0 °C in an ice water bath. An excess of tetrafluoroboric acid diethyl ether adduct ($HBF_4 \bullet Et_2O$, 50-55% v/v) was added drop-wise to the cold amine. A white precipitate immediately formed. The reaction was allowed to stir for ~1 h at 0 °C. The white precipitate was collected on a fritted glass funnel and washed with room temperature ether (3 x 10 mL) to remove excess $HBF_4 \bullet Et_2O$. The acid salt was transferred to a Schlenk flask and dried under vacuum at room temperature overnight to yield the acid as a white to off-white solid in near quantitative yields. When necessary, additional purification was performed by recrystallization from THF/pentane at –35 °C under an argon atmosphere.

Physical Methods. Electronic absorption spectra were recorded in a 1 cm cuvette on an 8453 Agilent UV-Vis spectrometer equipped with an Unisoku Unispeks cryostat. X-band (9.28 GHz) EPR spectra were collected as frozen solutions using a Bruker EMX spectrometer equipped with an ER041XG microwave bridge. Mössbauer spectra were recorded with a Janis Research Super-Varitemp dewar. Isomer shifts are reported relative to Fe metal at 298 K. Product(s) were detected by gas-chromatography mass spectrometry (GC-MS) in the Mass Spectrometry Facility at the University of California, Irvine. The GC-MS was a Trace MSplus from Thermo Fisher (San Jose, CA) using a 30m long x 0.25 mm i.d. DB-5 column from Agilent JW Scientific (Santa Clara, CA). The oven was held at 50°C for 1 minute then heated at a rate of 10°C min^{-1} to 290°C and held for an additional 35 minutes. The mass spectrometry used electron ionization (70 eV) scanning (1/sec) from m/z 50-650. Estimation of product yield was determined using an HP-6890 gas chromatograph with a flame ionization detector (FID) and a

30 m × 0.32 mm (5% phenyl)-methylpolysiloxane (0.25 ⌈m coating) capillary column (J&W Scientific DB-5) and helium carrier gas. The oven was held at 50°C for 1 minute then heated at a rate of 10°C min^{-1} to 290°C and held for an additional 5 minutes. Cyclic voltammetric experiments were conducted using a CHI600C electrochemical analyzer. A 2.0 mm glassy carbon electrode was used as the working electrode at scan velocities 0.01 $V{\cdot}s^{-1}$. A pentamethylferrocenium/pentamethylferrocene couple (-0.48 V vs. $[FeCp_2]^{+/0}$) was used as an internal reference to monitor the reference electrode (Ag^+/Ag).[4] The ^{57}Fe nuclear resonance vibrational spectroscopy (NRVS) data were recorded using published procedures on multiple occasions at beamline 3-ID at the Advanced Photon Source (APS).[6,7] he incident flux provided by the beamline is ~2 x 10^9 photos/s in a 1 meV bandwidth centered at 14.4125 keV in a 1 mm (vertical) x 3 mm (horizontal) spot. The monochromators used in the experiment consisted of a water-cooled diamond (1,1,1) double crystal with 1.1 eV bandpass, followed by two separate Si(4,0,0) and Si(10,6,4) channel-cut crystals in a symmetric geometry. During the measurements, samples were maintained at low temperatures using a closed-cycle helium cryostat. The temperature for individual spectra were calculated using the ratio of anti-Stokes to Stokes intensity according to $S(-E) = S(E) \exp(-E/kT)$ and were generally in the range of 40 K to 80 K. Spectra were recorded between -40 meV and 120 meV in 0.25 meV steps. Delayed nuclear fluorescence and iron K fluorescence (from internal conversion) were recorded with a single avalanche photodiode detector (APD) with 1 cm^2 detection area. Each scan required about 50 minutes, and all scans were added and normalized to the intensity of the incident beam. The ^{57}Fe partial vibrational density of state (PVDOS) was extracted from the raw NRVS data using the PHOENIX software package.[8]

XAS experiments were performed at the Stanford Synchrotron Radiation Laboratory (SSRL) on beam line 7-3 at 10 K. Fe K-edge data was collected using a Si(220) φ=0° double-crystal monochromator with a 9.0 keV cutoff for harmonic rejection. Soller slits were used in conjunction with an Mn filter. Data was collected in fluorescence mode with a Canberra 30-element Ge solid-state detector. To limit photoreduction of the samples, only first scans were

averaged into the final data sets (exposure time ~35 minutes). Fe K-edge data for the both the $Fe^{III}OH$ and $Fe^{IV}O$ species was comprised of 11 first scans, while the data sets for the $Fe^{IV}O(H)$ species contained 30 first scans. Energies were calibrated using an iron foil (7111.2 eV) and edge energies were obtained from the first derivative of the data with 1.0 eV smoothing and a third order polynomial in the program EXAFSPAK.

The Fe K-edge data sets were fit over the region k=1-16 $Å^{-1}$ using EXAFSPAK[9] with *ab initio* phases and amplitudes generated with the program FEFF v8.40.[10] The Fe K-edge fits for the three iron species were comprised of the first and second shell atoms as well as one multiple scattering component. In all cases, the second shell atoms included the carbon atoms neighboring the equatorial and axial nitrogen atoms (N=9, 6, and 4 for $Fe^{III}OH$, $Fe^{IV}O$, and $Fe^{IV}O(H)$, respectively) and in the case of the $Fe^{IV}O(H)$ species, the arm nitrogen atoms (N=3) were included. The Fe-N-C-Fe multiple scattering pathway involving the surrounding nitrogen atoms and their nearest neighbor carbon atom was included for the $Fe^{III}OH$ and $Fe^{IV}O$ species (N=12 and 18, respectively), however was omitted from the $Fe^{IV}O(H)$ fit in favor of the second shell N_{arm} scattering which had a greater contribution to the scattering. All Debye-Waller factors were treated as free parameters. The scale factor, S_0, was set to 0.9. Monochromator glitches in the Fe K-edge data sets at approximately k=14.5 $Å^{-1}$ were removed using a cubic polynomial fit to the data. No other modifications to the raw data were performed.

DFT Calculations. The DFT calculations were performed with the program suite Gaussian '09.[11] The geometry optimizations were performed using the functional/basis set combination bp86/tzvp. The free energy differences reported in the main text were evaluated using Gibbs free energies obtained with the frequency keyword at 298 K. ΔE_Q and η were calculated with bp86/tzvp, using Q = 0.17 barn. The ^{57}Fe isomer shift δ was evaluated for electron densities obtained with single point bp86/6-311g calculations at bp86/tzvp optimized structures. Additional DFT calculations were performed using ADF[12,13] and QUILD[14] programs, following methods described previously.[15] Geometry optimizations and frequency calculations were performed using PBE-D_2/TZ2P,[16] with solvent (COSMO)[17-19] and relativistic (ZORA)[12,20]

effects included self-consistently. Mössbauer parameters were obtained with S12g/TZ2P using parameters for the isomer shift specific for this combination of density functional and basis set (unpublished data).

Reactivity Studies of $[Fe^{IV}H_3buea(O)]^-$ (2) at Low Temperature using UV-vis Spectroscopy. For a typical experiment, a stock solution of $[Fe^{IV}H_3buea(O)]^-$ (**2**) at ~1-2 mM concentration (2 mg, 0.004 mmol) was prepared in of THF (15 mL) with 1.5 equiv 18-crown-6 ether (2 mg, 0.01 mmol) and stored at −36 °C. The concentration of **2** was determined using the extinction coefficient at λ_{max} = 550 nm (ε = 3000 $M^{-1}cm^{-1}$). To a 1 cm cuvette was added 2 mL of metal complex solution. The cuvette was sealed with a rubber septum then transferred to the precooled UV-vis spectrometer and allowed to equilibrate for at least 20 minutes at –80 °C under a flow of argon gas. Stock solutions of reactants were prepared by dissolving 10 mg in 1 mL of the appropriate solvent generating solutions between 20-40 mM. Solutions of reagents were then injected via gas-tight syringe and the progress of the reaction monitored optically.

Oxidation of 2 in the Presence of a Phenol. A stock solution of **2** was prepared in THF as described above. Stock solutions of phenol, either 2,4,6-tri-*tert*-butylphenol (66 mg, 0.25 mmol) or 2,4-di-*tert*-butylphenol (56 mg, 0.25 mmol), were prepared in THF (250 μL). A stock solution of [N(*p*-tolyl)$_3$][OTf] was prepared by dissolving the deep blue solid (10 mg, 0.023 mmol) in THF (2 mL). A stock solution of diphenylhydrazine (DPH) was prepared by dissolving the solid (10 mg, 0.054 mmol) in THF (5 mL). A 2 mL aliquot of the solution of **(2)** was transferred to a 1 cm quartz cuvette and sealed with a rubber septum before cooling to –80 °C in the cryostat of the UV-vis spectrometer. To this solution, 100 equiv of phenol was added via gas-tight syringe and the mixture was allowed to stir for 1 min before injection of 1 equiv of [N(*p*-tolyl)$_3$][OTf]. Reactions with 2,4,6-tri-*tert*-butylphenol were monitored optically for the generation of **1** and 2,4,6-tri-*tert*-butylphenoxy radical (λ_{max} = 380 and 400 nm).

In the case of 2,4-di-*tert*-butylphenol, the generation of **1** was monitored by the growth of the absorbance band at 540 nm, requiring ~60 seconds, and then treated with 0.5 equiv of DPH to quench the reaction. The reaction was deemed complete after the complete loss of the

optical band of **1** at 540 nm. After completion, the solution was transferred at room temperature in air from the cuvette into a 1.8 mL vial for analysis using GC-MS. Product yield was calculated from GC using a calibration curve generated for pure **10**. ESI^+ m/z *Anal* (calc): *410.45* ($C_{28}H_{42}O_2$ 410.32)

Control Reaction of 1 with Phenol. Stock solutions of **2**, phenol, and DPH prepared as described above. A solution of $[H_3NPh][BF_4]$ was prepared by dissolving the white solid (10 mg, 0.055 mmol) in THF (2 mL). To a solution of **2** precooled to –80 °C was added 1 equiv $[H_3NPh][BF_4]$ and the reaction was monitored optically for the generation of **1**. Upon complete generation of **1**, 100 equiv of phenol were added and in the case of 2,4,6-tris-*tert*-butylphenol were monitored optically: the peaks associated with **1** were unchanged and the peaks associated with the generation of 2,4,6-tris-*tert*-butylphenoxy radical (λ_{max} = 380 and 400 nm) were not observed. After 90 seconds, the typical reaction time for complimentary oxidation reactions, 0.5 equiv of DPH were added and the decrease of the band at 540 nm was monitored to observe quenching of the reaction. After reaction completion, in the case of 2,4-di-*tert*-butylphenol, the contents of the cuvette were transferred at room temperature in air to a 1.8 mL vial and subjected to analysis by GC-MS. We did not observe any species associated with oxidized organic products.

Control Reaction of 2 with Phenol. Stock solutions of **2** and phenol prepared as described above. To a solution of **2** precooled to –80 °C in a 1 cm cuvette was added 100 equiv of 2,4,6-tris-*tert*-butylphenol. The reaction mixture was monitored optically for the generation of 2,4,6-tris-*tert*-butylphenoxy radical (λ_{max} = 380 and 400 nm) coupled with the decrease in absorbance bands associated with the **2** complex. After 120 seconds, the typical reaction time for complimentary oxidation reactions, 0.5 equiv of DPH were added and the decrease of the band at 550 and 800 nm were monitored to determine quenching of the reaction. After reaction completion, in the case of 2,4-di-*tert*-butylphenol, the contents of the cuvette were transferred at room temperature in air to a 1.8 mL vial and subjected to analysis by GC-MS.

Control Reaction of [N(*p*-tolyl)$_3$][OTf] and Phenol. Stock solutions of [N(*p*-tolyl)$_3$][OTf]

and 2,4,6-tris-*tert*-butylphenol prepared as described above. To a solution of [N(*p*-tolyl)$_3$][OTf] (2 mL, 100-200 μM) precooled to –80 °C was added 100 equiv of phenol. The mixture was monitored optically for 120 seconds for the decrease of the bands associated with [N(*p*-tolyl)$_3$][OTf] and the generation of 2,4,6-tri-*tert*-butylphenoxy radical.

Note: The formation of the TBP radical was not observed for the control experiments that used 2,4,6-tris-*tert*-butylphenol with **2** and [N(*p*-tolyl)$_3$][OTf] during the timeframe of the reactions (Figure S14).

Preparation of Mössbauer Samples of 1 with ^{57}Fe. The same procedure described above was used to generate **1** at 3 mM concentration in THF using ~96% ^{57}Fe-enriched **2** with a few exceptions. Inside the cryostat of a UV-vis spectrometer, 2 mL of 3 mM, ^{57}Fe-enriched **2** was cooled to –100 °C. The rubber septum sealing the cuvette was quickly removed with the aid of a razor blade under a flow of argon gas. The precooled solution was then treated with either oxidant or acid solution and monitored for the disappearance of the low energy band for **2** at 800 nm (ε = 300 M^{-1}cm^{-1}). After ~30 seconds, the cuvette was removed from the cryostat and its contents were quickly poured into liquid nitrogen. The resulting frozen solution was then packed into pre-cooled Mössbauer cups for analysis.

Preparation of NRVS Samples for 2. A 10 mM solution of 96% ^{57}Fe-enriched **2** (10 mg, 0.02 mmol) was prepared in THF (2 mL) with 18-crown-6 ether (6 mg, 0.02 mmol) added for increase solubility. The concentration of **2** was determined by UV-vis spectroscopy as described above for the preparation of Mössbauer samples by transferring a portion of the solution to a 1 mm path length cuvette. A NRVS sample holder was cooled in the cold well of a drybox to -196 °C. To the pre-cooled NRVS sample holder, a sample of **2** (500 μL of the 10 mM solution) was added via syringe and allowed to freeze completely. The sample was then transferred from the drybox and quickly placed in a container pre-cooled to 77K. Samples were analyzed for purity using Mössbauer spectroscopy prior to, and after NRVS data collection. Solution NRVS sample holders were prepared from Mössbauer sample holders by cutting a 2 x 6 mm slot out of the

bottom and covering the hole with kapton tape.

Preparation of NRVS Samples for 1. The same general procedure described above for the preparation of NRVS samples of **2** was used to prepare those of **1** with the following modifications. A 10 mM solution of **2** in THF was transferred to a cuvette and placed inside a cryostat of a UV-vis spectrometer pre-cooled to –100 °C. The rubber septum sealing the cuvette was quickly removed with the aid of a razor blade under a flow of argon gas. The pre-cooled solution was then treated with a solution of $[H_3NPh][BF_4]$ (40 μL, 0.5 M in THF) added via gas-tight syringe and monitored for the disappearance of the low energy band for **2** at 800 nm (ε = 300 $M^{-1}cm^{-1}$). After ~30 s, the cuvette was removed from the cryostat and its contents were rapidly poured into liquid N_2. The resulting frozen solution was transferred into a pre-cooled NRVS sample holder and packed by carefully thawing and refreezing the frozen solution under a stream of argon gas. Samples were analyzed for purity using Mössbauer spectroscopy prior to, and after NRVS data collection.

Preparation of Low-Temperature EPR Samples. A solution of **2** (~15 mM, 250 μL) was transferred to an EPR tube and sealed with a rubber septum. The tube was brought out of the dry box and placed in a −95 °C methanol/liquid nitrogen bath and allowed to equilibrate for five minutes. Stock solutions of reactant prepared as described above were added via a syringe. After mixing by careful shaking of the tube, the EPR tube was quickly removed from the cold bath, wiped clean of methanol, and frozen in liquid nitrogen before analysis.

Preparation of Low-Temperature Solution XAS Samples of 2. Solution XAS samples were prepared in a similar manner as solution NRVS samples described above with the following modifications: a 10 mM solution of **2** (10 mg, 0.02 mmol), of which 2 mM was prepared with 96% ^{57}Fe-enriched **2**, was prepared in THF (2 mL) with 18-crown-6 ether (6 mg, 0.02 mmol) added for increase solubility. The concentration of **2** was determined by UV-vis spectroscopy as described above for the preparation of Mössbauer samples by transferring a portion of the solution to a 1 mm path length cuvette. A XAS sample holder was cooled in a cold well of a drybox to -196 °C. To the pre-cooled XAS sample holder, a sample of **2** (500 μL of

the 10 mM solution) was added via syringe and allowed to completely freeze. The sample was then transferred from the drybox and quickly placed in a container pre-cooled to 77 K. Samples were analyzed for purity using Mössbauer spectroscopy prior to XAS data collection. Solution XAS sample holders were prepared from Mössbauer sample holders by cutting off the bottom and covering the hole with kapton tape.

Preparation of Low-Temperature Solution XAS samples of 1. The same general procedure described above for the preparation of XAS samples of **2** was used to prepare those of **1** with the following modifications: a 10 mM solution of **2**, of which 2 mM was enriched with 96% ^{57}Fe-enriched **2**, in THF was transferred to a cuvette and placed inside a cryostat of a UV-vis spectrometer pre-cooled to –100 °C. The rubber septum sealing the cuvette was quickly removed with the aid of a razor blade under a flow of argon. The pre-cooled solution was then treated with a solution of $[H_3NPh][BF_4]$ (40 μL, 0.5 M in THF) via gas-tight syringe and monitored for the disappearance of the low energy band for **2** at 800 nm (ε = 300 $M^{-1}cm^{-1}$). After ~30 s, the cuvette was removed from the cryostat and its contents were rapidly poured into liquid N_2. The resulting frozen solution was transferred into a pre-cooled XAS sample holder and packed by carefully thawing and refreezing the frozen solution under a stream of argon. Samples were analyzed for purity using Mössbauer spectroscopy prior to XAS data collection.

Table S1. Best fits for EXAFS data.

	Fe-O			Fe-N_{eq}			Fe-N_{ax}				
Intermediate	N	R	σ^2	N	R	σ^2	N	R	σ^2	E_0	Error
4	1	1.85	0.00070	3	2.02	0.00329	1	2.26	0.00266	1.4	0.299
2	1	1.67	0.00273	4	2.00	0.00362	0	----	------	0.2	0.305
1	1	1.65	0.00331	3	1.96	0.00519	0	----	------	-4.7	0.330

Table S2. Best fits for Fourier filtered EXAFS data.

	Fe-O			Fe-N_{eq}			Fe-N_{ax}				
Intermediate	N	R	σ^2	N	R	σ^2	N	R	σ^2	E_0	Error
4	1	1.84	0.00112	3	2.00	0.00372	1	2.30	0.00616	-0.4	N/A
2	1	1.67	0.00246	4	2.00	0.00372	0	----	------	-0.1	N/A
1	1	1.65	0.00337	3	1.96	0.00514	0	----	------	-5.0	N/A

Table S3. DFT Computed Properties for the Optimized Tautomers **1a**-**1c**.

	1a	**1b**	**1c**
Fe1–O1, Å	1.703	1.696	1.812
Fe1–N1, Å	2.056	2.074	2.098
Fe1–N2, Å	2.062	2.118	1.919
Fe1–N4, Å	1.962	1.956	1.938
Fe1–N6, Å	1.963	1.962	2.025
O1…O2, Å	2.495	–	–
O1…H1, Å	1.450	1.549	0.989
O2…H1, Å	1.056	–	–
O2–C10, Å	1.319	1.238	1.243
N2–C10, Å	1.329	1.322	1.384

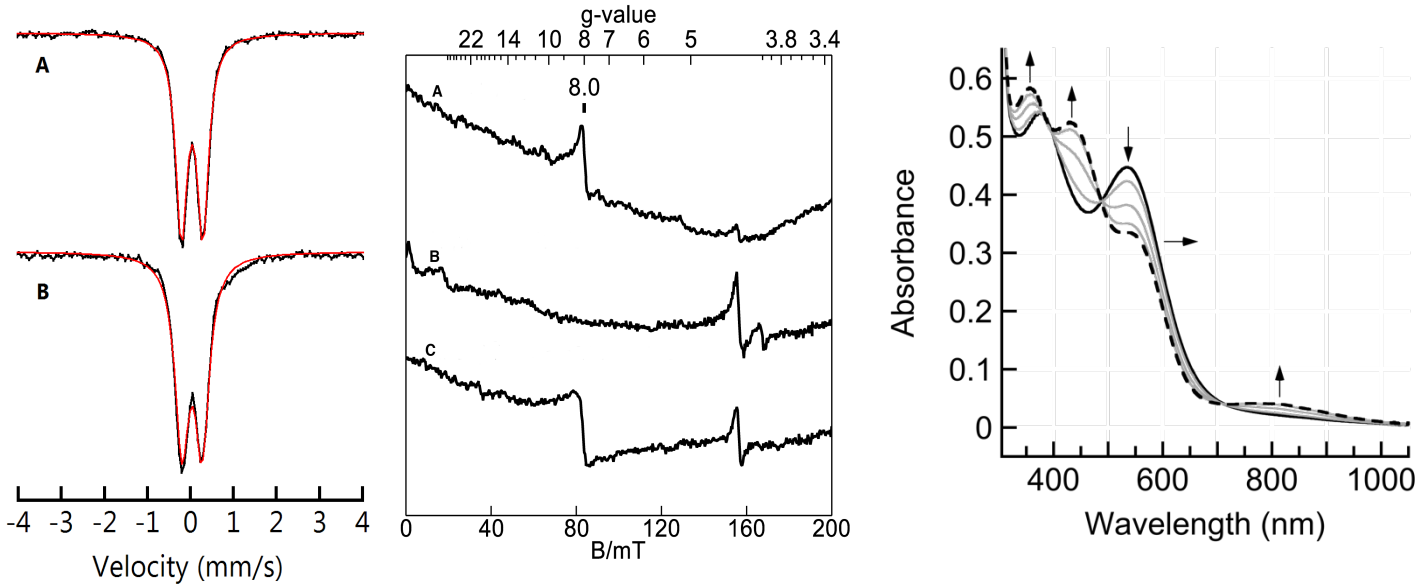

Figure S1. (Left) Mössbauer spectra of **2** (**A**) and **2** prepared from the deprotonation of **1** (**B**) recorded at 4 K in THF. Black lines are the least-square fits of the experimental data with linewidths: (**A**) 0.32 mm/s, (**B**) 0.40 mm/s. (Middle) Parallel-mode EPR spectra of **2** (**A**), after addition of $\{H_3NPh\}^+$ (**B**), and the after treating with DBU (**C**). (Right) Absorbance spectra of **1** (A) and after treating with increments of 0.25 equiv of DBU to convert back to **2** (**B**).

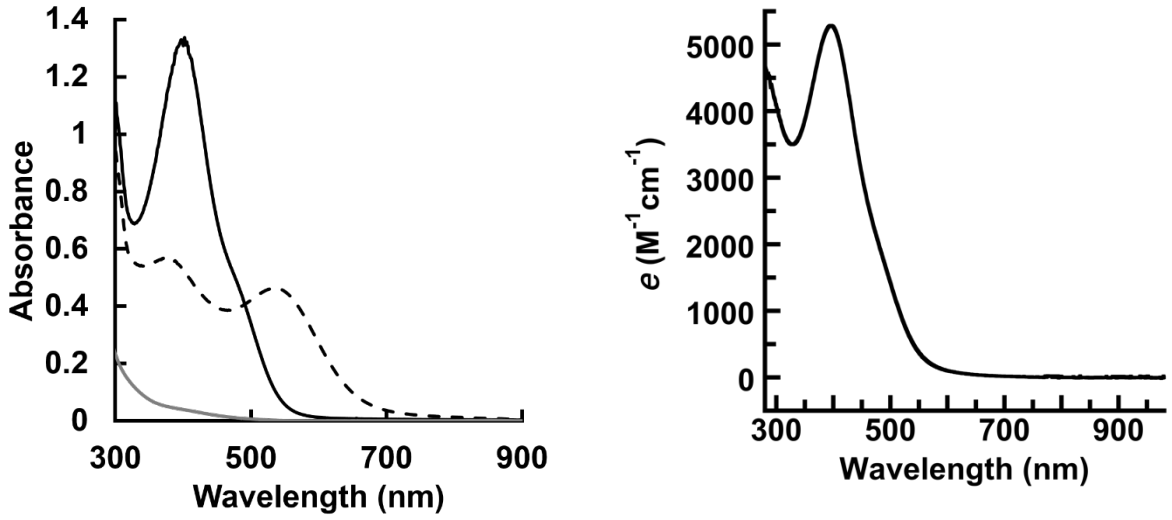

Figure S2. (Left) Absorbance spectra showing the reaction of **1** (dashed) with an equimolar amount of **3** (gray) to produce two equivalents of **4** (solid) recorded at –80 °C in THF. (Right) Absorbance spectrum for **4** recorded at room temperature in THF.

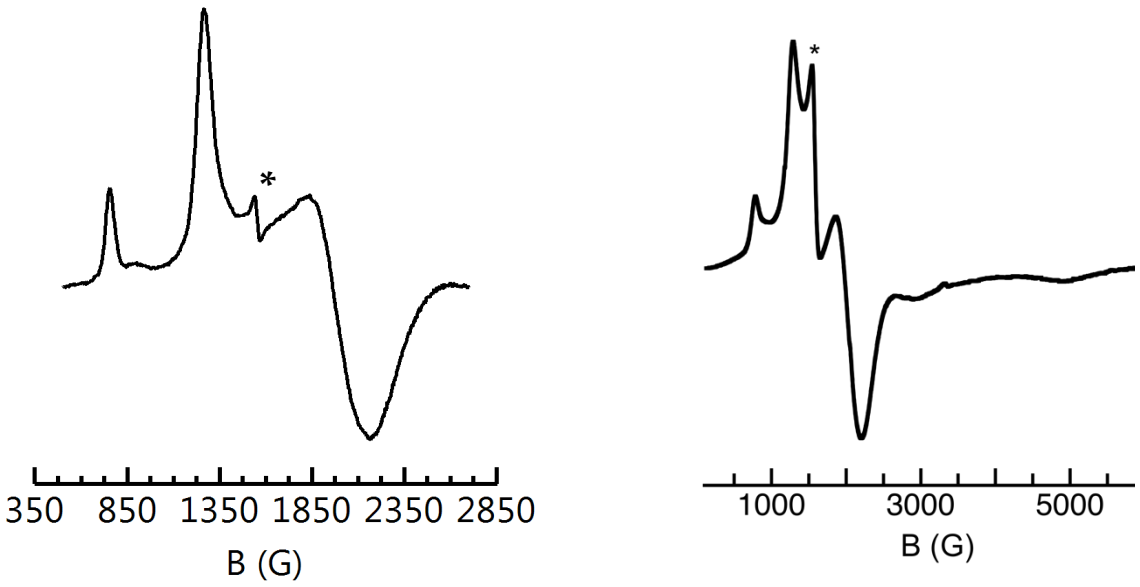

Figure S3. (Left) EPR spectrum of the comproportionation of **1** with **3** to generate **4**, recorded at X-band, 77 K, power 2 mW, frozen solution in THF. (Right) EPR spectrum of **4**. Asterisk denotes an adventitious ferric species.

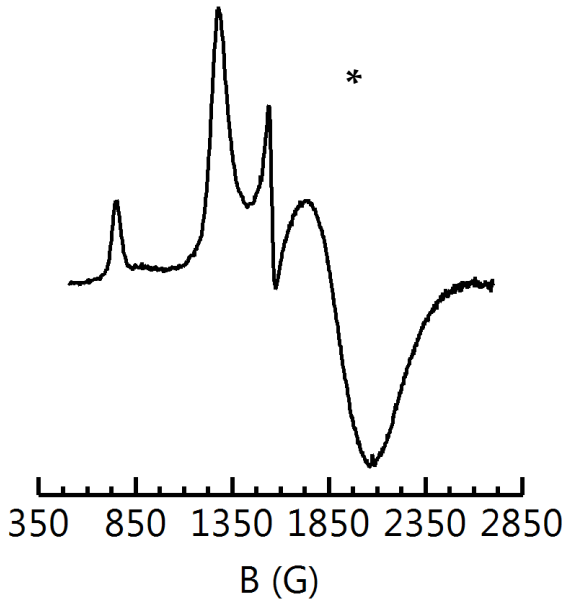

Figure S4. EPR spectrum of the reduction of **1** with [$CoCp_2$] to generate **4**, recorded at X-band, 77 K, power 6 mW, frozen solution in THF. Asterisk denotes an adventitious ferric species. Reactions were done at -80˚C in THF under Ar.

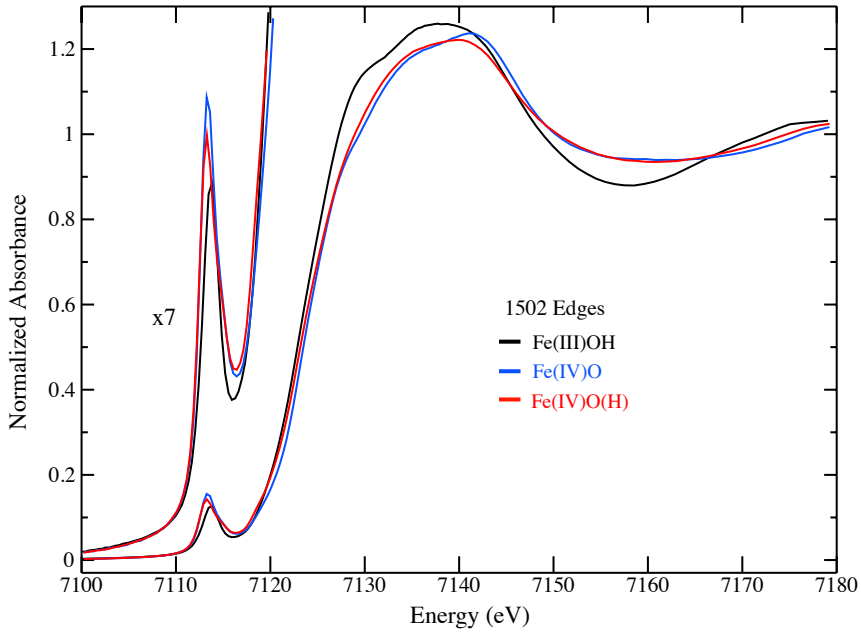

Figure S5. XANES spectra for **1** (red), **2** (blue), and **4** (black).

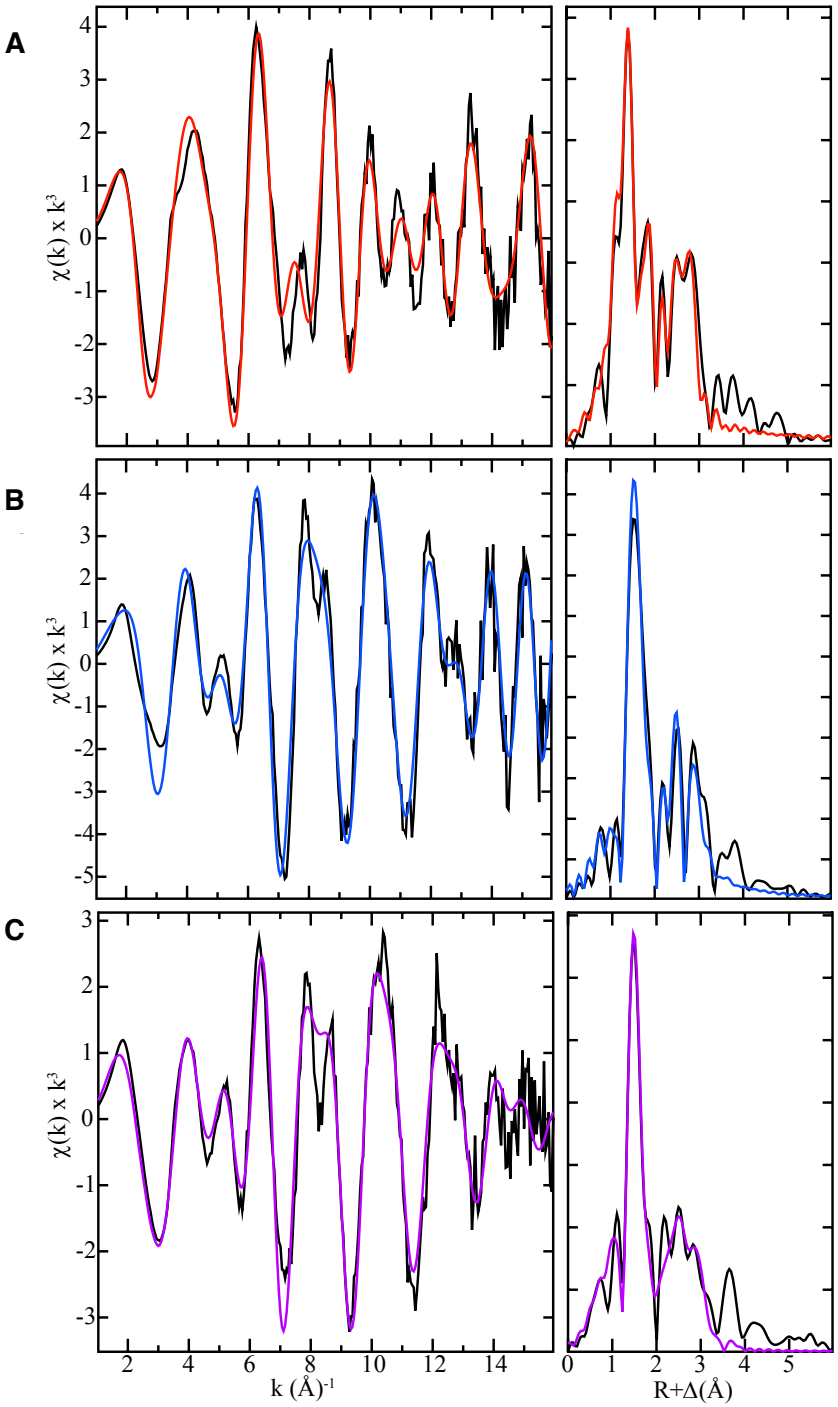

Figure S6. EXAFS data (left) and the Fourier transforms (right) for **4** (**A**), **2** (**B**), and **1** (**C**).

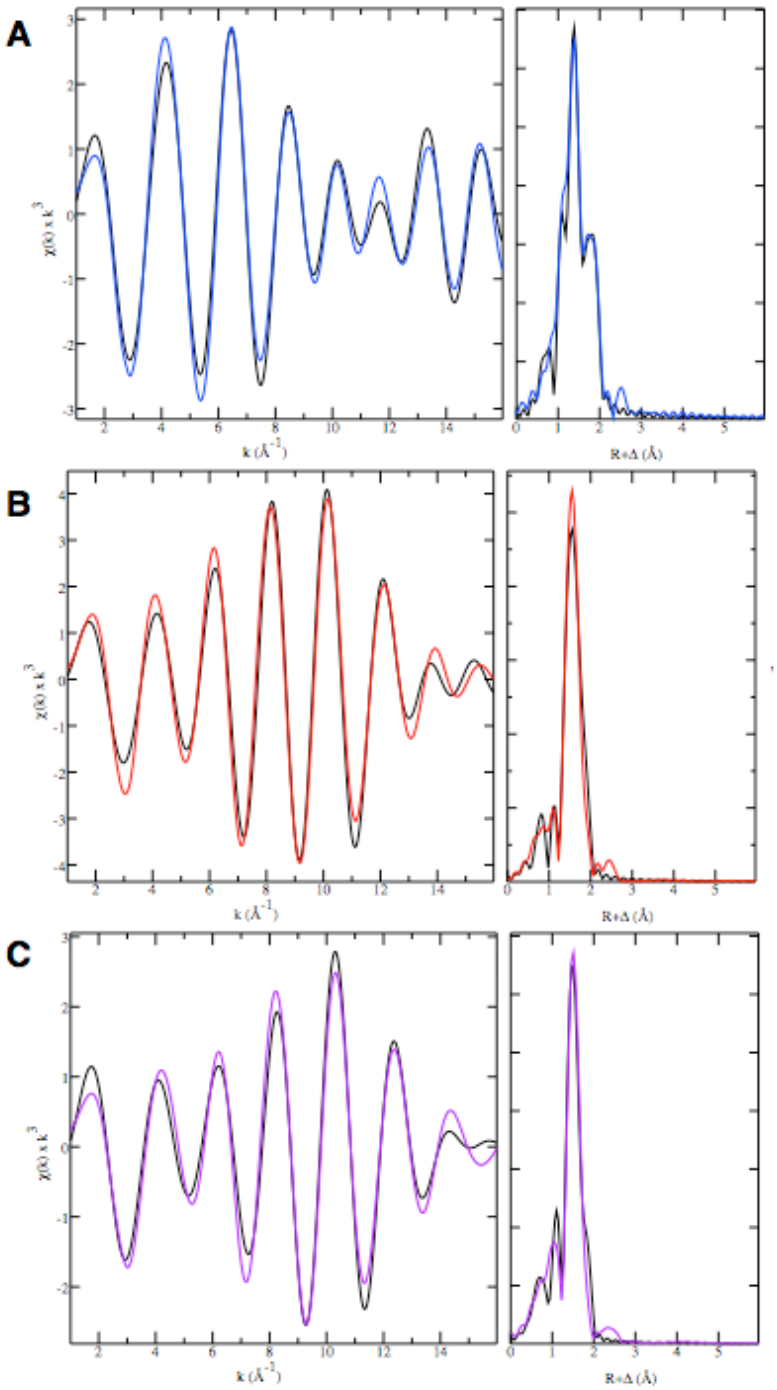

Figure S7. Fourier filtered EXAFS data (left) and the Fourier transforms (right) for **4** (**A**), **2** (**B**), and **1** (**C**).

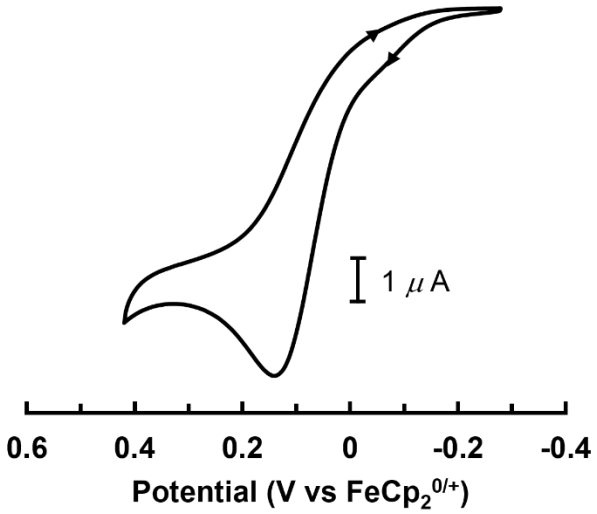

Figure S8. Cyclic voltammogram of **2** collected in THF at room temperature (with 0.1 M TBAP).

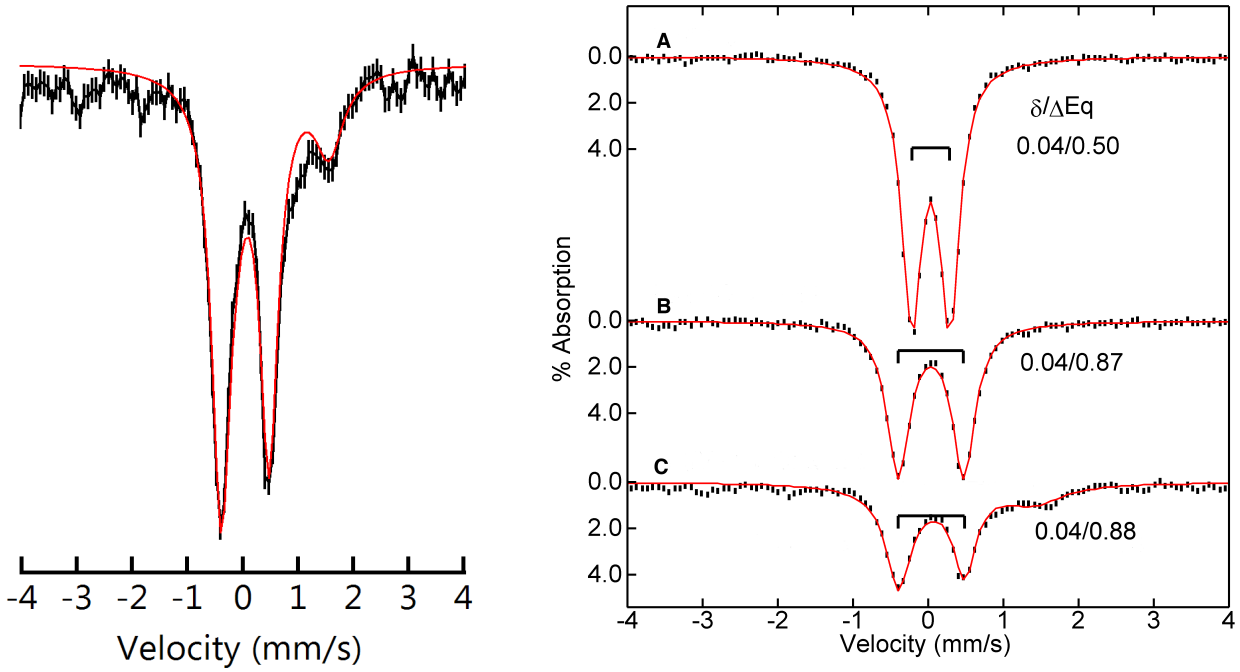

Figure S9. (Right) Mössbauer spectrum of the reaction of **2** with N(*p*-tolyl)$_3^{+\bullet}$ in THF at –100 °C. Spectrum collected at 4 K. Black trace is the least-square fit of the experimental data. The major doublet (δ = 0.04 mm/s, ΔE_Q = 0.87 mm/s, linewidth 0.40 mm/s) matches **1** and the minor doublet (δ = 0.65 mm/s, ΔE_Q = 1.83 mm/s, linewidth 0.62 mm/s) is an unknown ferric impurity. (Left) Comparison of Mössbauer spectra for **2** (**A**) and **1** prepared with $[H_3NPh]^+$ (**B**) and with N(*p*-tolyl)$_3^{+\bullet}$ (**C**).

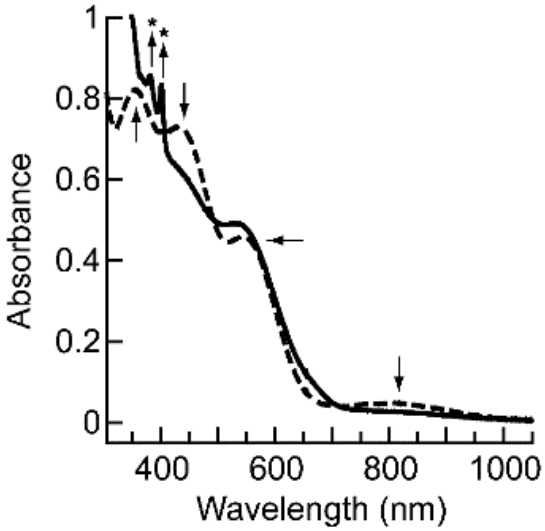

Figure S10. Experimental evidence for the reaction shown in eq 3: electronic absorbance spectra for the oxidative conversion of **2** (dash) to **1** (solid) with **1** equiv of $N(p\text{-tol})_3^{+\bullet}$ and 100 equiv of **7** recorded at -80˚C in THF. The starred peaks are from 2,4,6-tri-*tert*-butylphenoxy radical, **9**.

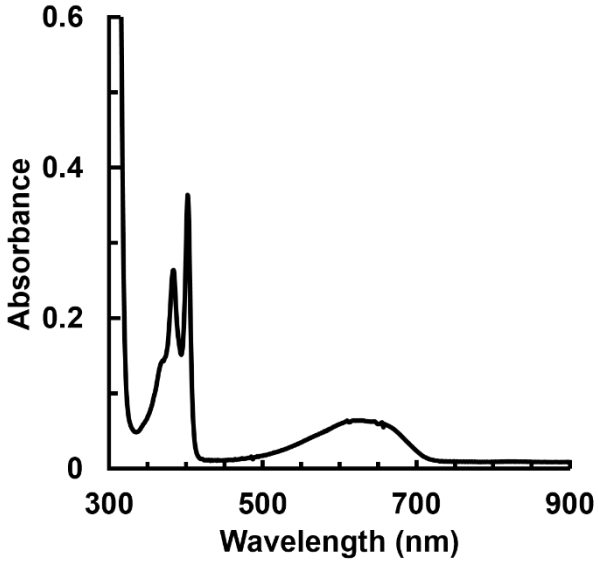

Figure S11. Electronic absorption spectrum of a 10 μM solution of independently prepared tri-tertbutylphenoxy radical (**9**) in THF recorded at –80 °C.

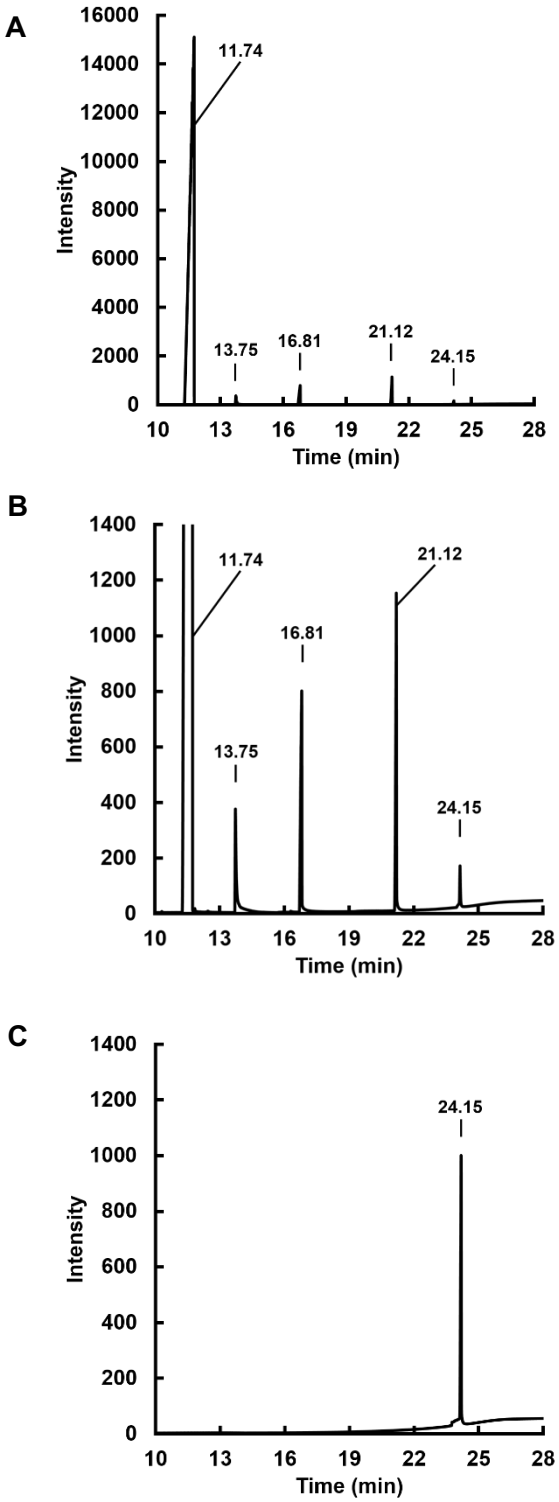

Figure S12. Gas chromatograms (GC) of the oxidation of **2** in the presence of 100 equiv **8**. The full GC (**A**), the expanded GC showing the peaks with larger retention times (**B**), and the GC for **10** (**C**). Key: **8**, (11.74 min), excess DPH (13.75 min), m 18-crown-6 ether (16.81 min), N(*p*-tolyl)$_3$ (21.12 min), and **10** (24.15 min).

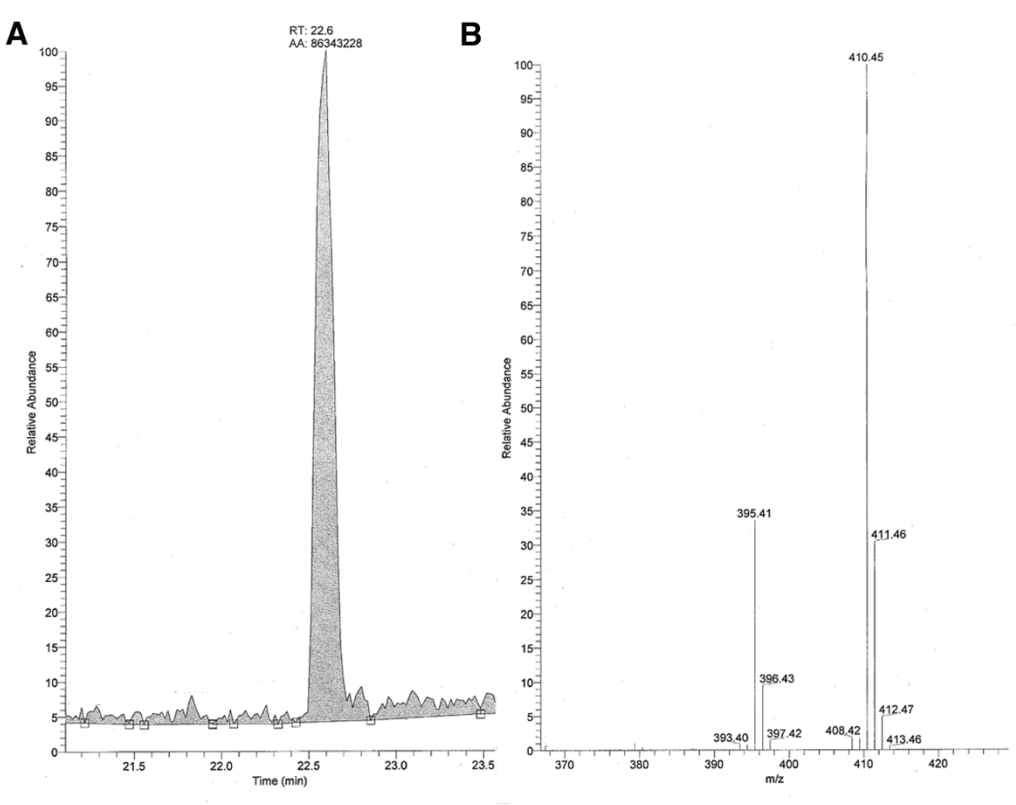

Figure S13. The GC trace (**A**) and matching MS trace (**B**) for the oxidation of **2** in the presence of 100 equiv **8**. MS trace shows **10** at m/z = 410.45 and m/z for **10**$(-CH_3)^+$ = 395.41.

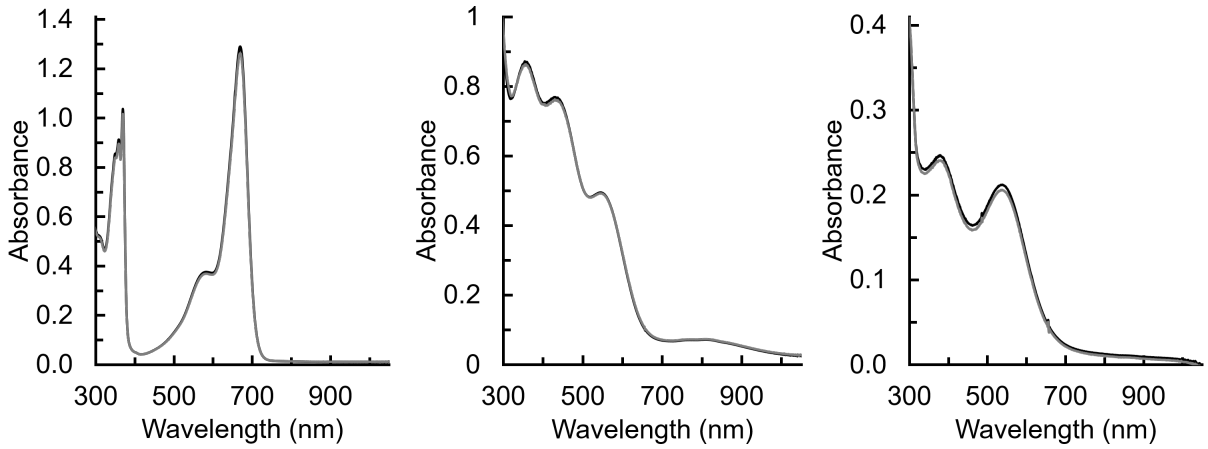

Figure S14. Optical results from: (left) control reaction of **2** with 2,4,6-tris-*tert*-butylphenol, (middle) control reaction of [N(*p*-tolyl)$_3$][OTf] with 2,4,6-tris-*tert*-butylphenol, (right) control reaction of **1** with 2,4,6-tris-*tert*-butylphenol. Reactions were done at –80 °C in THF. Key: the starting spectrum (black) and 120 s after addition of 2,4,6-tris-*tert*-butylphenol (gray). The reaction time was 90 s for the spectra on the right.

References.

(1) Lacy, D. C.; Gupta, R.; Stone, K. L.; Greaves, J.; Ziller, J. W.; Hendrich, M. P.; Borovik, A. S. *J. Am. Chem. Soc.* **2010**, *132*, 12188–12190.
(2) Shirin, Z.; Hammes, B. S.; Young, V. G.; Borovik, A. S. *J. Am. Chem. Soc.* **2000**, *122*, 1836–1837.
(3) MacBeth, C. E.; Hammes, B. S.; Victor G. Young, J.; Borovik, A. S. *Inorg. Chem.* **2001**, *40*, 4733–4741.
(4) Connelly, N. G.; Geiger, W. E. *Chem. Rev.* **1996**, *96*, 877–910.
(5) Kanamura, K.; Yonezawa, S.; Kawai, Y.; Takehara, Z.-I. *J. Electroanal. Chem. Interfacial Electrochem.* **1991**, *301*, 291–295.
(6) Sturhahn, W. *J. Phys. Condens. Matter* **2004**, *16*, S497–S530.
(7) Toellner, T. S. *Hyperfine Interact.* **2000**, *125*, 3–28.
(8) Sturhahn, W. *Hyperfine Interact.* **2000**, *125*, 149–172.
(9) Gearge, G. N. EXAFSPAK, 2000.
(10) Ankudinov, A. L.; Ravel, B.; Rehr, J. J.; Conradson, S. D. *Phys. Rev. B* **1998**, *58*, 7565–7576.
(11) Frisch, M. J.; Trucks, G. W.; Schlegel, H. B.; Scuseria, G. E.; Robb, M. A.; Cheeseman, J. R.; Scalmani, G.; Barone, V.; Mennucci, B.; Petersson, G. A.; Nakatsuji, H.; Caricato, M.; Li, X.; Hratchian, H. P.; Izmaylov, A. F.; Bloino, J.; Zheng, G.; Sonnenberg, J. L.; Hada, M.; Ehara, M.; Toyota, K.; Fukuda, R.; Hasegawa, J.; Ishida, M.; Nakajima, T.; Honda, Y.; Kitao, O.; Nakai, H.; Vreven, T.; Montgomery Jr., J. A.; Peralta, J. E.; Ogliaro, F.; Bearpark, M.; Heyd, J. J.; Brothers, E.; Kudin, K. N.; Staroverov, V. N.; Keith, T.; Kobayashi, R.; Normand, J.; Raghavachari, K.; Rendell, A.; Burant, J. C.; Iyengar, S. S.; Tomasi, J.; Cossi, M.; Rega, N.; Millam, J. M.; Klene, M.; Knox, J. E.; Cross, J. B.; Bakken, V.; Adamo, C.; Jaramillo, J.; Gomperts, R.; Stratmann, R. E.; Yazyev, O.; Austin, A. J.; Cammi, R.; Pomelli, C.; Ochterski, J. W.; Martin, R. L.; Morokuma, K.; Zakrzewski, V. G.; Voth, G. A.; Salvador, P.; Dannenberg, J. J.; Dapprich, S.; Daniels, A. D.; Farkas, O.; Foresman, J. B.; Ortiz, J. V.; Cioslowski, J.; Fox, D. J. Gaussian 09, 2010.
(12) te Velde, G.; Bickelhaupt, F. M.; Baerends, E. J.; Fonseca Guerra, C.; van Gisbergen, S. J. A.; Snijders, J. G.; Ziegler, T. *J. Comput. Chem.* **2001**, *22*, 931–967.
(13) Baerends, E. J.; Ziegler, T.; Autschbach, J.; Bashford, D.; Berger, A.; Bérces, A.; Bickelhaupt, F. M.; Bo, C.; de Boeij, P. L.; Boerrigter, P. M.; Borini, S.; Bulo, R. E.; Cavallo, L.; Chong, D. P.; Deng, L.; Dickson, R. M.; van Duin, A. C. T.; Ellis, D. E.; Faassen, M. v.; Fan, L.; Fischer, T. H.; Fonseca Guerra, C.; Ghysels, A.; Giammona, A.; van Gisbergen, S. J. A.; Götz, A. W.; Groeneveld, J. A.; Gritsenko, O. V.; Grüning, M.; Gusarov, S.; Harris, F. E.; Heine, T.; van den Hoek, P.; Jacob, C. R.; Jacobsen, H.; Jensen, L.; Kadantsev, E. S.; Kaminski, J. W.; van Kessel, G.; Klooster, R.; Kootstra, F.; Kovalenko, A.; Krykunov, M. V.; van Lenthe, E.; Louwen, J. N.; McCormack, D. A.; McGarrity, E.; Michalak, A.; Mitoraj, M.; Neugebauer, J.; Nicu, V. P.; Noodleman, L.; Osinga, V. P.; Patchkovskii, S.; Philipsen, P. H. T.; Post, D.; Pye, C. C.; Ravenek, W.; Rodríguez, J. I.; Romaniello, P.; Ros, P.; Schipper, P. R. T.; Schreckenbach, G.; Seldenthuis, J. S.; Seth, M.; Skachkov, D. G.; Snijders, J. G.; Solà, M.; Swart, M.; Swerhone, D.; te Velde, G.; Vernooijs, P.; Versluis, L.; Visscher, L.; Visser, O.; Wang, F.; Wesolowski, T. A.; van Wezenbeek, E. M.; Wiesenekker, G.; Wolff, S. K.; Woo, T. K.; Yakovlev, A. L. ADF, 2012.
(14) Swart, M. *J. Chem. Theory Comput.* **2008**, *4*, 2057–2066.
(15) Swart, M. *Chem. Commun.* **2013**, *49*, 6650.
(16) Perdew, J. P.; Burke, K.; Ernzerhof, M. *Phys. Rev. Lett.* **1996**, *77*, 3865–3868.
(17) Klamt, A.; Schüürmann, G. *J. Chem. Soc., Perkin Trans. 2* **1993**, 799–805.
(18) Pye, C. C.; Ziegler, T. *Theor. Chem. Acc.* **1999**, *101*, 396–408.
(19) Swart, M.; Rösler, E.; Bickelhaupt, F. M. *Eur. J. Inorg. Chem.* **2007**, *2007*, 3646–3654.
(20) Lenthe, E. van; Baerends, E. J.; Snijders, J. G. *J. Chem. Phys.* **1993**, *99*, 4597.